AD-A206 731 ULTRASMALL HOLOGRAPHIC X-RAY GRATINGS USING SYNCHROTRON RADIATION AND X-R (U) OREGON UNIV EUGENE INST OF THEORETICAL SCIENCE P L CSONKA ET AL NOV 88 1/1

UNCLASSIFIED AFOSR-TR-89-0415 AFOSR-87-0211 F/G 20/8 NL

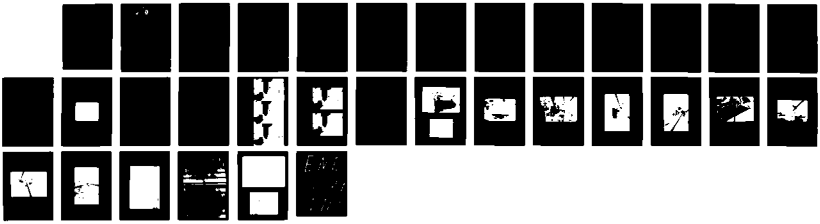

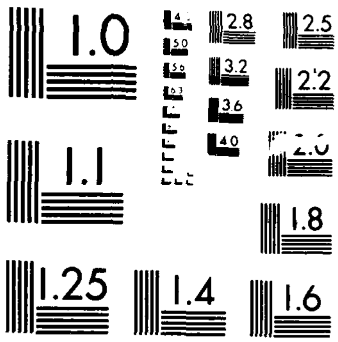
1.0
2.8
2.5
3.2
2.2
3.6
4.0
2.0
1.1
1.8
1.25
1.4
1.6

8c. ADDRESS (City, State, and ZIP Code)	10. SOURCE OF FUNDING NUMBERS			
Building 410, Bolling AFB DC 20332-6448	PROGRAM ELEMENT NO. 61102F	PROJECT NO. 2301	TASK NO. A1	WORK UNIT ACCESSION

11. TITLE (Include Security Classification)	(U) ULTRASMALL AND SUPERFINE HOLOGRAPHIC X-RAY GRATINGS USING SYNCHROTRON RADIATION AND X-RAY LITHOGRAPHIC TECHNIQUES
12. PERSONAL AUTHOR(S)	Csonka

13a. TYPE OF REPORT	13b. TIME COVERED	14. DATE OF REPORT (Year, Month, Day)	15. PAGE COUNT
FINAL	FROM 1 May 87 TO 30 Apr 88	Nov 1988	30

16. SUPPLEMENTARY NOTATION

17. COSATI CODES			18. SUBJECT TERMS (Continue on reverse if necessary and identify by block number)
FIELD	GROUP	SUB-GROUP	
	20.06		Grating, Lithography, Undulator ,

TECHNICAL REPORT

On Grant

AFOSR-TR- 89-0415

Titled: **"ULTRASMALL HOLOGRAPHIC X-RAY GRATINGS, USING SYNCHROTRON RADIATION AND X-RAY LITHOGRAPHIC TECHNIQUES"**

Grant Number: AFOSR-87-0211

Period Covered: May 1, 1987 to April 30, 1988

Report prepared by: Paul L. Csonka, Principal Investigator

and

Roman O. Tatchyn, Co-investigator

Institute of Theoretical Science

University of Oregon

Eugene, Oregon 97403-5203

Beam Line Characterization

In our series of experiments use was made of radiation generated by the undulator magnet,[1] transported from SSRL at Stanford, and recently installed on ALADDIN[2] at the Synchrotron Radiation Center (SRC) in Wisconsin. Since the properties of that radiation were not previously known, the first step consisted of characterizing the radiation not only spectrally, but also in angular intensity space.

The angular characterization was accomplished by allowing the radiation to pass through a pinhole[3] before reaching a gold photodiode. The photodiode measurements served to ascertain the beam profiles along both the horizontal and vertical directions.[4] In terms of the first harmonic frequency, ν_1, the first harmonic photon energy, ϵ_1, can be written as $h\nu_1$. At $h\nu_1$ = 50 eV, the measurements confirmed expectations and demonstrated a Gaussian distribution along both axes. Two sets of measurements were performed: one with, the other without interposition of an aluminum filter 800 Å thick. (See Fig. 1.) The results are displayed in Figs. 2 and 3. The absorption effects of aluminum can be observed at $h\nu_1$ = 90 eV in Fig. 4.

The undulator spectra were observed, as dispersed by a transmission grating, in the vicinity of the monochromator focal plane. The spectra have been photographed when the undulator was tuned such that $h\nu_1$ had the values 50, 60, 70, 80 and 90 eV. (Fig. 5a, b, c, d and e). Densitometer traces of the photographed spectra were taken, and are displayed in Fig. 6.

We appreciated the opportunity of being able to utilize the new undulator beamline at ALADDIN, before its public commissioning.

2. Monochromator Construction and Characterization

A transmission grating monochromator[5] was constructed and tested. The instrument is based on a 5000 lines/mm gold transmission grating operating at normal incidence. The optical configuration of the monochromator consisted of a bent cylindrical mirror (Fig. 7) refocusing the undulator photons onto an exit slit plane. The cylindrical mirror was located at a distance of 12.9 meters from the source, and the exit slit was 43 inches beyond that mirror. A transmission grating with a 2000 Å period was located 7 inches from the cylindrical mirror. The grating intercepted the radiation at normal incidence, and dispersed the focused orders in the vertical plane.

The cylindrical mirror consisted of a floatglass substratum which was gold-coated at the Synchrotron Radiation Center in Wisconsin. It was appropriately curved and aligned with the help of a He-Ne laser arranged in such a manner as to accurately reproduce the geometry of the synchrotron radiation beam to be used in the actual experiment. Figure 8 shows the spatial distribution of the focused laser light, along the vertical in the focal plane. The FWHM was measured to be 45 μm. During the alignment the deflection generated by the transmission grating was simulated by a special deflection mirror (Fig. 9), attached at the exit end of the cylindrical mirror assembly. Following the alignment the deflection mirror was replaced by the transmission grating, and the monochromator was assembled. A layout of the mechanical components is shown in Fig. 10. The photons generated inside the undulator are led through the differential pumping section to the UHV chopper.

That instrument[6] provides an attenuation of the photon beam intensity. The attenuation factor can be set anywhere in the range from 10^{-2} to unity, and is wavelength independent. The attenuated photon beam then proceeds to the bent cylindrical mirror, located in the mirror chamber. There the beam is refocused through the transmission grating onto the exit plane of the instrument. An end view of the mirror chamber with the mirror installed is shown in Fig. 10b. Figure 10c illustrates the system under vacuum with a phosphorized viewing screen attached. That screen facilitated viewing of the diffracted undulator spectra described in Sec. 1.

3. Interferometer Construction and Operation

A split beam interferometer previously designed and partially fabricated at SSRL, was completed at the Wisconsin Synchrotron Radiation Center. It contained two symmetrically placed grazing indicence mirrors, deflecting coherent radiation into PMMA samples. A view of the interferometer components is shown in Fig. 11, and a front view of the assembled device can be seen in Fig. 12. The adjustable aperture stop carriage provided a means for inserting an aperture stop or translucent objects into either of the two interferometer beams. When assembled, the gold coating on the reference alignment crystal (Fig. 11) is normal to the plane bisecting the interferometer's horizontal aperture, and is used to assist in aligning the orientation of the interferometer crystal surfaces with respect to the monochromator output axis. The alignment was accomplished using He-Ne laser light. The assembled interferometer was installed inside a specially constructed chamber, with provisions for continuously aligning the position and attitude of the interferometer box. A side view of this chamber with the interferometer installed is shown in Fig. 13. The complete monochromator-interferometer beamline can be seen on Fig. 14, as viewed from the downstream end.

The vibration environment was characterized with an accelerometer and spectrum analyzer, and it was determined that there were no motion components with amplitudes in excess of 300 Ångstroms. The exposures showed perceptible patterns defined by the interferometer geometry. Interference fringes associated with Fresnel diffraction of the interferometer mirrors were recorded.

4. Monochromator Operation

The monochromator assembly was operated for approximately 60 hours. The operation was predominantly with the undulator first harmonic energy tuned to 50 eV. The average total radiation input power was approximately 3 Watts. Over the approximately 60 hour period of operation the chopper attenuation factor was varied from close to 6% to unity. The estimated total power impinging on the grating was close to 1.0 Watt. The vacuum inside the chamber was kept at about 2.10^{-7} Torr during the entire duration of the experiment. Following these exposures, damage to the transmission grating as well as carbon contamination of the cylindrical mirror and the grating were observed.

A photograph of the grating prior to its installation is displayed in Fig. 15. Photographs of the damaged area are shown in Figs. 16a and 16b. A study of damage mechanisms in transmission gratings irradiated with synchrotron light[6] indicates that a primary damage mechanism in such gratings is associated with differential expansion of the bars, generated by the inhomogeneous temperature profile of the irradiated structure. Based on such studies the damage threshold is to be expected in the vicinity of 1.0 Watt/cm^2, which is consistent with the observed effect.

The observed carbon contamination on the cylindrical mirror, as can be seen on Fig. 17, was consistent with prior observations of carbon contamination of synchrotron radiation optics in relatively poor vacuum.

5. Interference Experiment and Results.

A. Coherent Power

The exposure times utilized in the experiment were based on the estimated vertical coherent power, $P_{v,coh}$ (0.1%), provided by the new undulator at the Synchrotron Radiation Center in Wisconsin. One has

$$P_{v,coh}(0.1\%) = \frac{1}{4\pi^2} \frac{1}{\sigma_y \sigma_{y'}} P_{tot}(0.1\%) \frac{c}{2\nu_1} \eta_{grating} \eta_{chopper},$$

where P_{tot} (0.1%) is the total power at the first harmonic frequency, ν_1, within a frequency interval $\Delta\nu = 10^{-3}\nu_1$, while $\eta_{grating}$ and $\eta_{chopper}$ are the grating and chopper transmission efficiencies respectively. One also has

$\sigma_y' = 1.19.10^{-4}$rad , $\sigma_x' = 3.49.10^{-4}$rad ,

$\sigma_y = 1.42.10^{-2}$rad cm , $\sigma_x = 1.49.10^{-1}$rad cm .

At the selected photon energy of 50 eV, the nominal sensitivity of PMMA is augmented by about an order of magnitude (due to the decreased photon penetration depth) to about 0.1 Joules/cm^2. Based on such considerations, exposures were taken in the range of 8 to 16 hours.

B. Modes of Operation

Plans called for operating the interferometer in two distinct modes. The first of these was equivalent to a Lloyd's mirror mode of operation with an asymmetrically positioned aperture stop. In the second mode of operation the aperture stop was to be centrally positioned, so as to obtain an interference pattern in the center of the resist.

C. Results

So far the instrument was operated only in the Lloyd's mirror configuration. Irrespective of the exposure time (within the limits quoted above) perceptible patterns were recorded (Fig. 18). This was consistent with visual observations of fluorescence on the phosphorized aperture stop, which indicated that the monochromator was properly aligned with respect to the exposed resist. The observed patterns contain easily discernible Fresnel fringes associated with diffraction off the edge of the interferometer mirror. The long period, λ_F, of the Fresnel pattern is corroborated exactly by the wavelength of the monochromatized light and the distance, L, from the edge of the mirror to the resist, via the formula

$$\lambda_F = \sqrt{L\lambda_1} .$$

In addition to the above, a much weaker periodic pattern was also observed, but due to the low contrast ratio we were so far not able to confidently identify those with an interference pattern generated by the primary interferometer beams.

6. Future Experiments

So far we have not performed experiments in the second interferometer mode of operation, because of a lack of time on the beamline. It is our intention to perform such experiments either at SSRL or at SRC. We are confident that this can be accomplished within the next few months.

The instrument assembly has been designed so as to have the capability of taking x-ray holograms of objects located in either branch of the interfering beams. It is therefore a logical next step in the sequence of experiments to be performed with this instrument. Indeed, we were hoping to obtain one more set of exposures after the original expiration date of this grant, during a period of no-cost extension. Our request for such an extension having been turned down, we intend to proceed with those experiments after the expiration date of the present grant period.

7. Take-off Mirror

The preparation at SSRL of a takeoff mirror for BL V is continuing. It is projected that one of the major applications of this take-off station will be to operate the experimental system as described above, and tested in Wisconsin. The take-off mirror design is based on multilayer technology, and has been finalized. The vacuum chamber was completed in 1987, and the mirror blank is presently in the process of being polished.

References

1) H. Winick and G. Brown, "Wiggler and Undulator Magnets - an Overview," NIM 195, (1982) 347.

2) Storage ring at the Synchrotron Radiation Center (SRC) in Wisconsin.

3) R. Tatchyn, P. Csonka, H. Kilic, H. Watanabe, A. Fuller, M. Beck, A. Toor, J. Underwood, R. Catura, "Focusing of undulator light at SPEAR with a lacquer-coated mirror to power densities of 10^9 Watts/cm^2," SPIE Proceedings 733, (1986) 368.

4) R.O. Tatchyn, M. Green, T. Cremer, E. Kallne, A. Toor and P. Csonka, "Photodiode Characterization of the Undulator Beam Profile at ALADDIN," to be published.

5) E. Kallne, R.O. Tatchyn, P.L. Csonka, I. Lindau, "Applications of Transmission X-Ray Optics," NIM A 246, (1986) 327.

6) R. Tatchyn, R. Boyce, "A UHV Chopper Design for SSRL," NIM 222, (1984) 345.

7) R.O. Tatchyn, J.T. Cremer, P.L. Csonka, E. Kallne and A. Toor, "Operation of a Normal Incidence Transmission Grating Monochromator at ALADDIN," reported at the Third International Conference on Synchrotron Radiation Instrumentation, Tsukuba, Japan, 1988.

Figure Captions

Fig. 1 800 Å thick Aluminum foil supported by an 85% transmitting Ni metal mesh.

Fig. 2 Undulator radiation intensity distribution along the vertical axis when $h\nu_1$ = 50 eV, (a) with, and (b) without the Aluminum filter present in the beam.

Fig. 3 Undulator radiation intensity distribution along the horizontal axis when $h\nu_1$ = 50 eV, (a) with, and (b) without the Aluminum filter present in the beam.

Fig. 4 Vertical undulator radiation intensity distribution for $h\nu_1$ = 90 eV with the Aluminum filter located in the beam.

Fig. 5 Five photographs (a, b, c, d and e) of the undulator spectrum for first harmonic energy $h\nu_1$ = 50, 60, 70, 80 and 90 eV.

Fig. 6 Densitometer trace of undulator spectra when $h\nu_1$ = 50 eV(a), 60 eV (b), 70 eV (c), 80 eV (d), 90eV (e).

Fig. 7 Gold coated cylindrical floatglass mirror (in monochromator).

Fig. 8 Vertical intensity distribution of He-Ne laser light focused on the monochromator focal plane.

Fig. 9 Optical deflection mirror mounted at the exit of the cylindrical mirror assembly.

Fig. 10 (a) Mechanical layout of the monochromator assembly (b) End view of the chamber containing the cylindrical mirror. (c) Chamber containing the cylindrical mirror, with an appended nipple to provide a phosphorized screen for viewing diffracted undulator spectra, immediately upstream from monochromator exit plane.

Fig. 11 View of the interferometer components.

Fig. 12 Front view of the assembled interferometer.

Fig. 13 A specially constructed chamber holding the interferometer (visible through viewports).

Fig. 14 View of the complete monochromator - interferometer beamline. The observer is located at the downstream end of the interferometer.

Fig. 15 Transmission grating prior to installation.

Fig. 16 (a) Photographs of the damaged area on the transmission grating surface, after exposure to radiation inside the interferometer. (b) Photograph showing the transition between damaged and undamaged areas of the exposed grating. The undamaged area is located directly above a Si substratum, which shields it from radiation.

Fig. 17 Carbon contamination on a cylindrical mirror surface after approximately 60 hours of exposure.

Fig. 18 Typical interference pattern recorded with the interferometer in the Lloyd's mirror mode of operation.

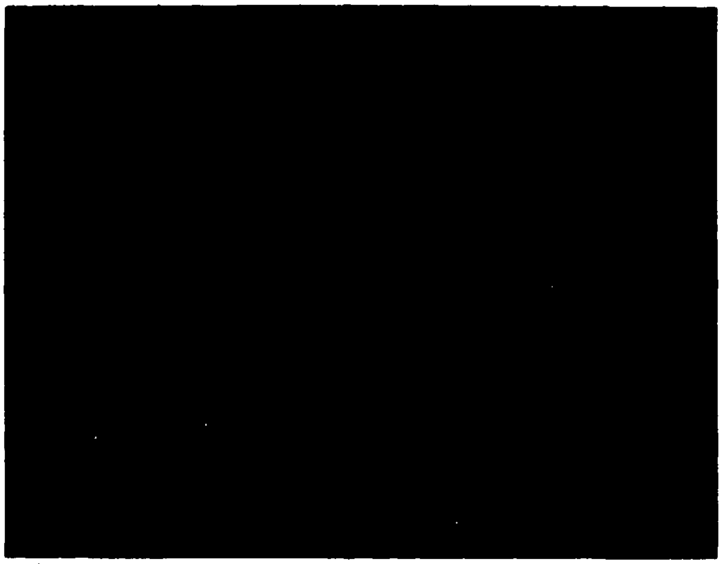

Figure 1

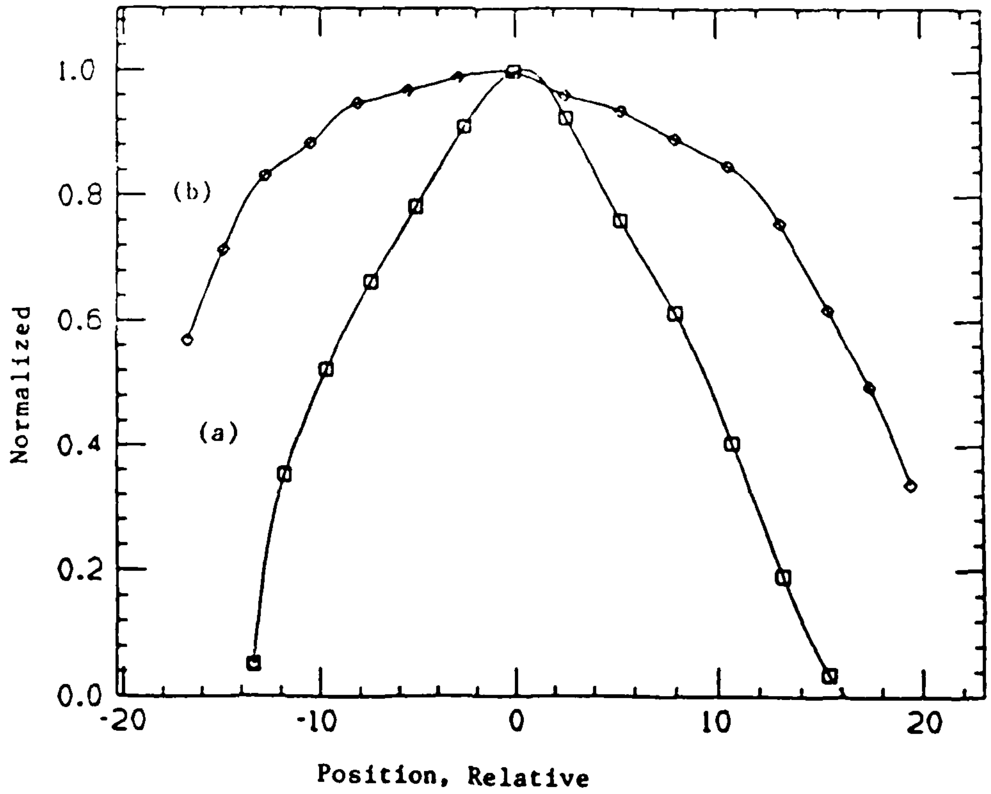

Figure 2

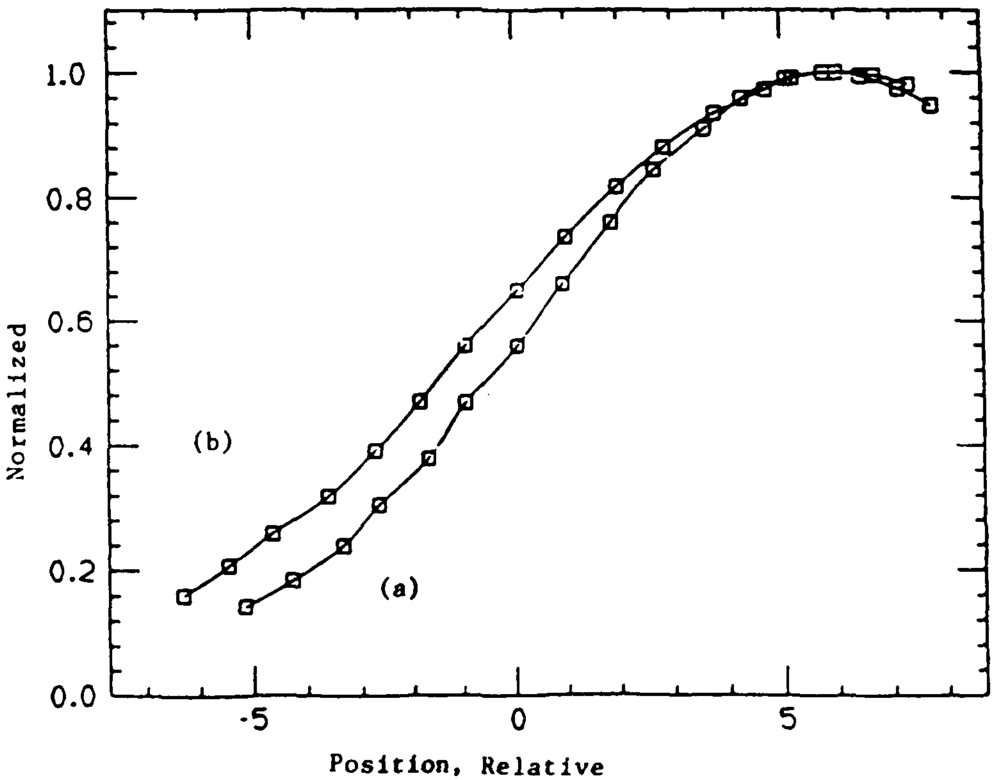

Figure 3

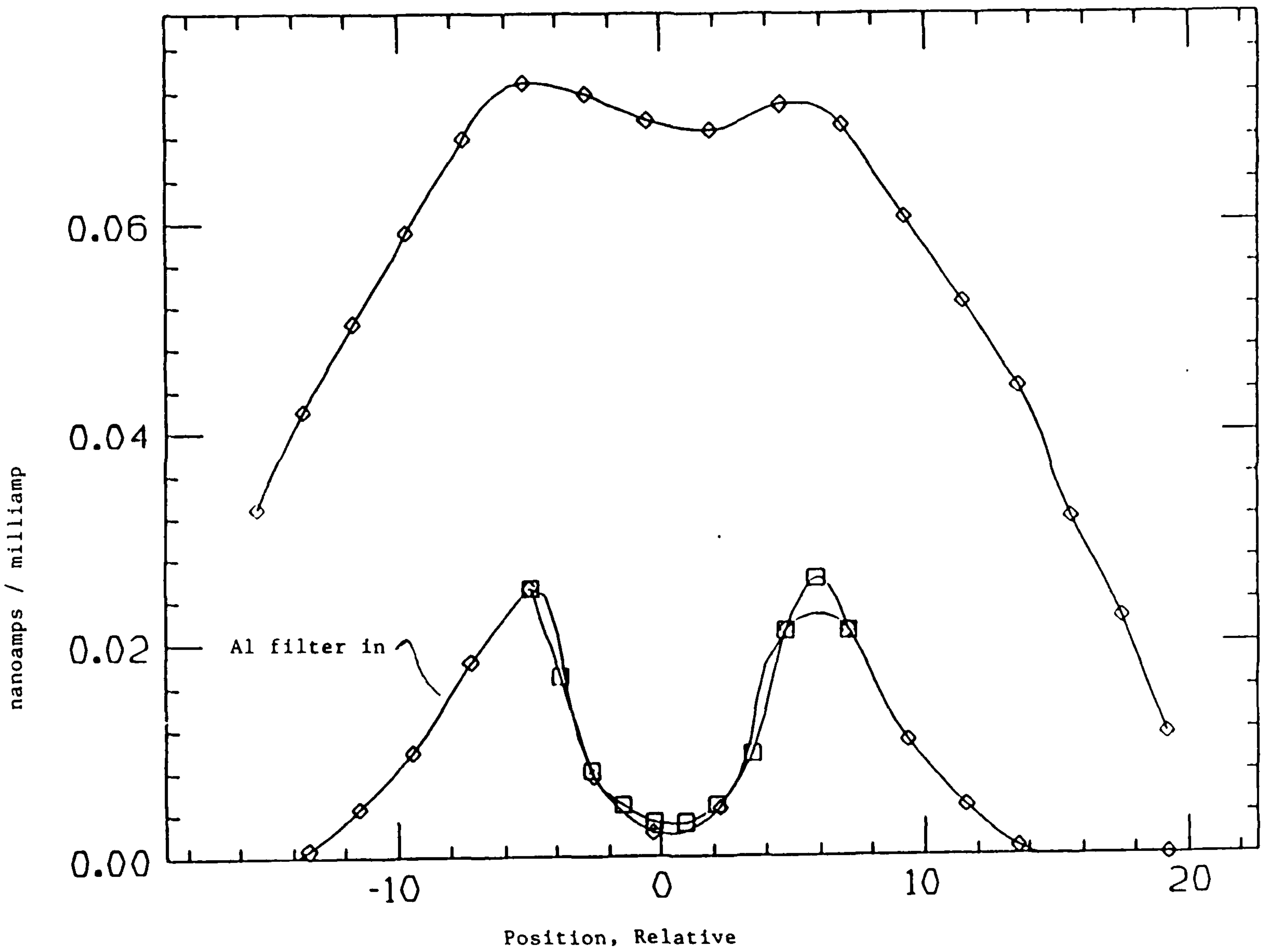
0.06
0.04
0.02
0.00
-10
0
10
20
Position, Relative
nanoamps / milliamp
Al filter in

Figure 4

Figure 5a

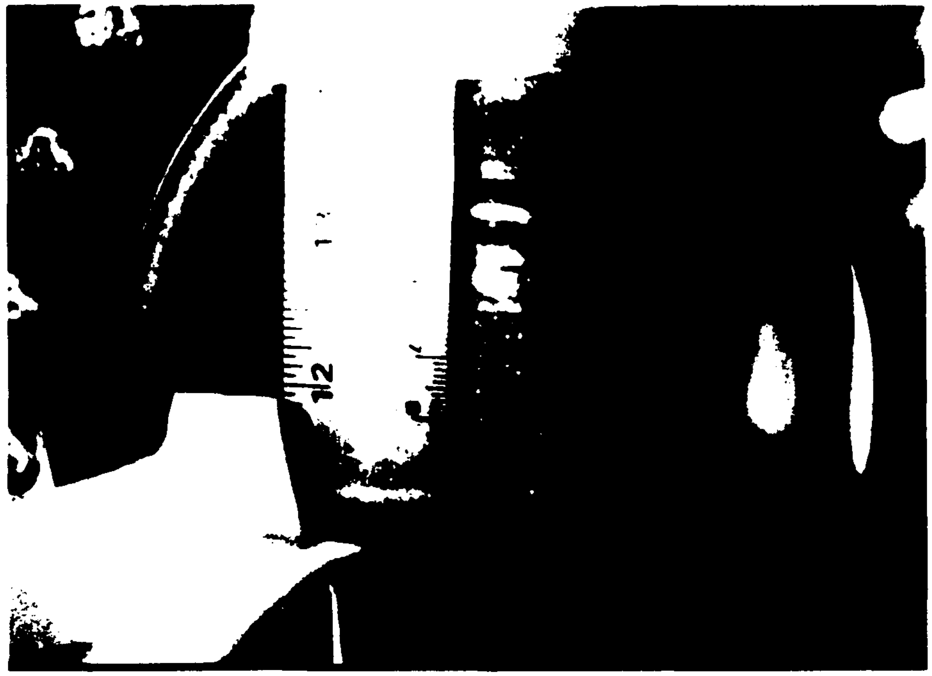

Figure 5b

Figure 5c

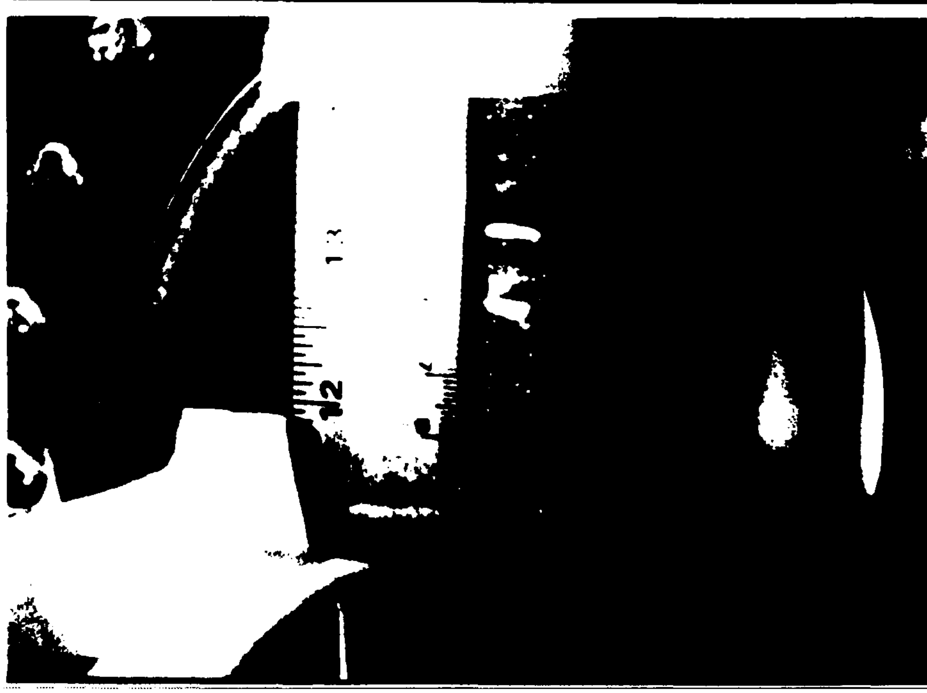

Figure 5d

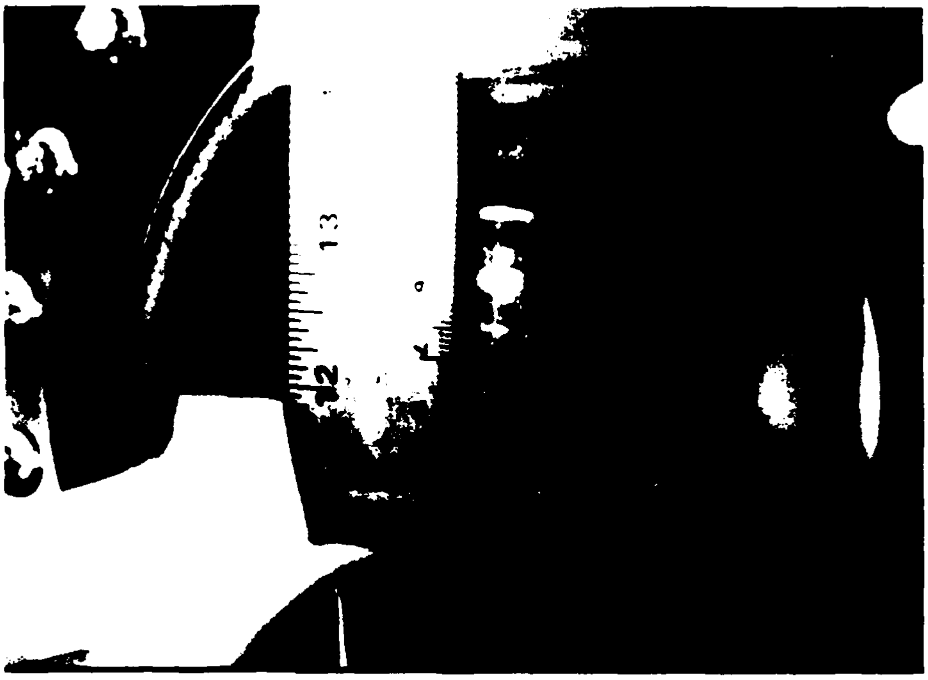

Figure 5e

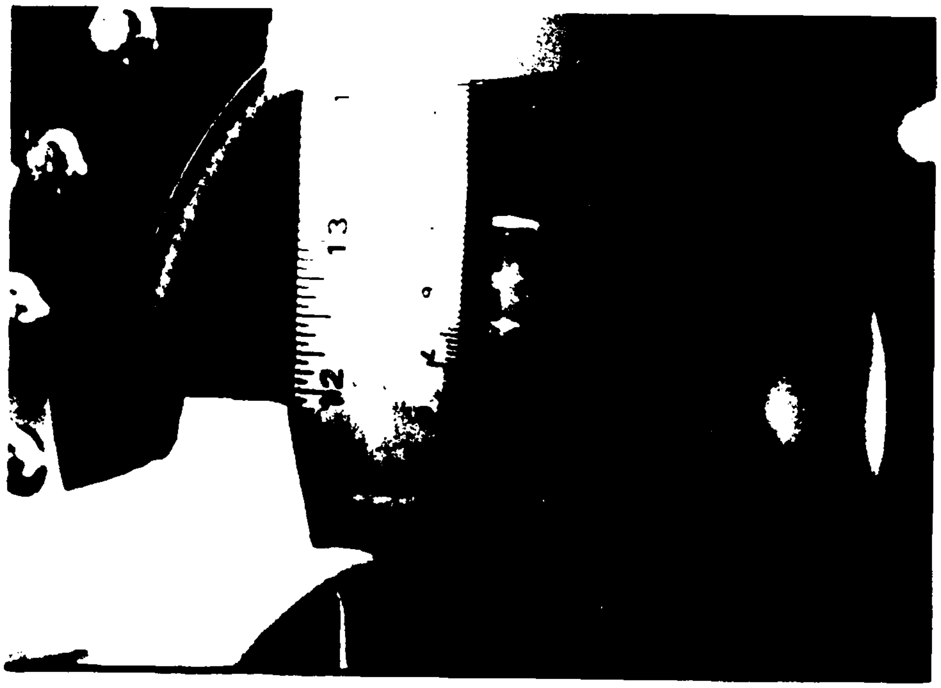

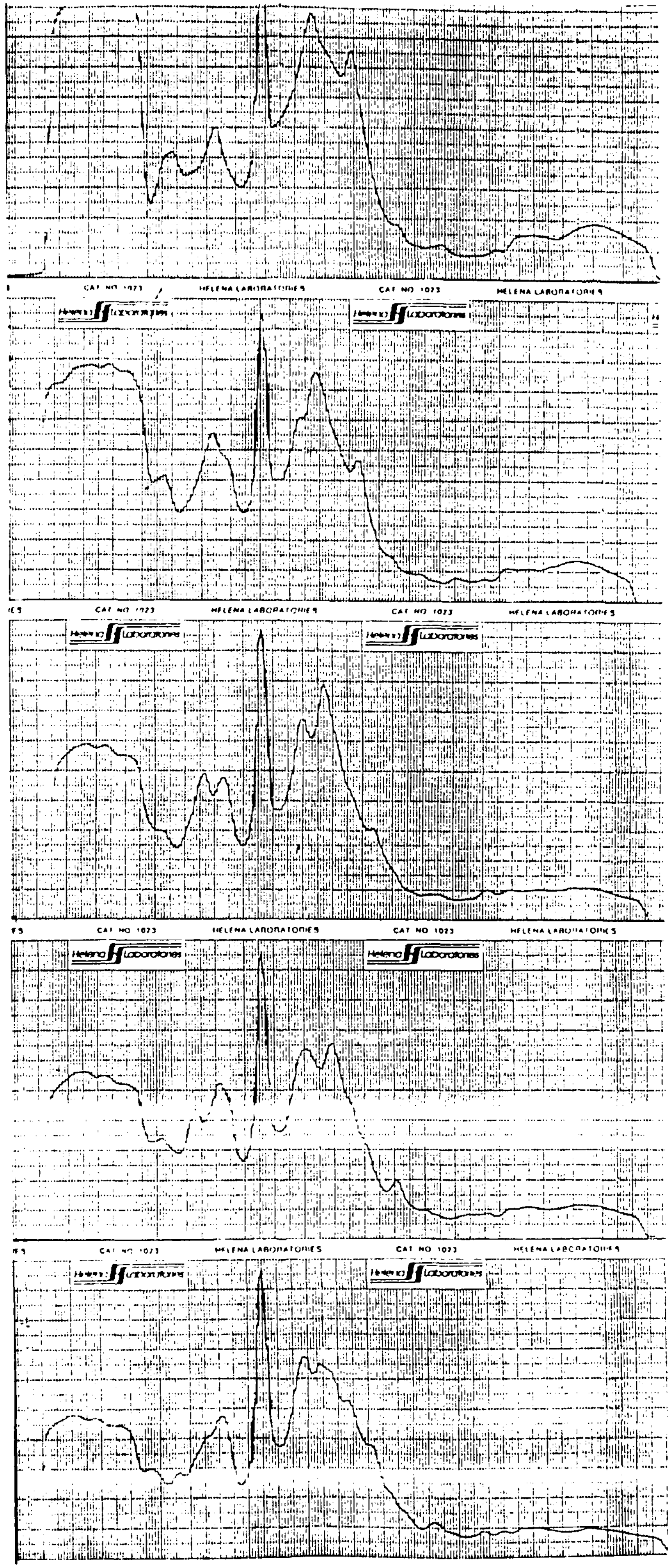

Figure 6

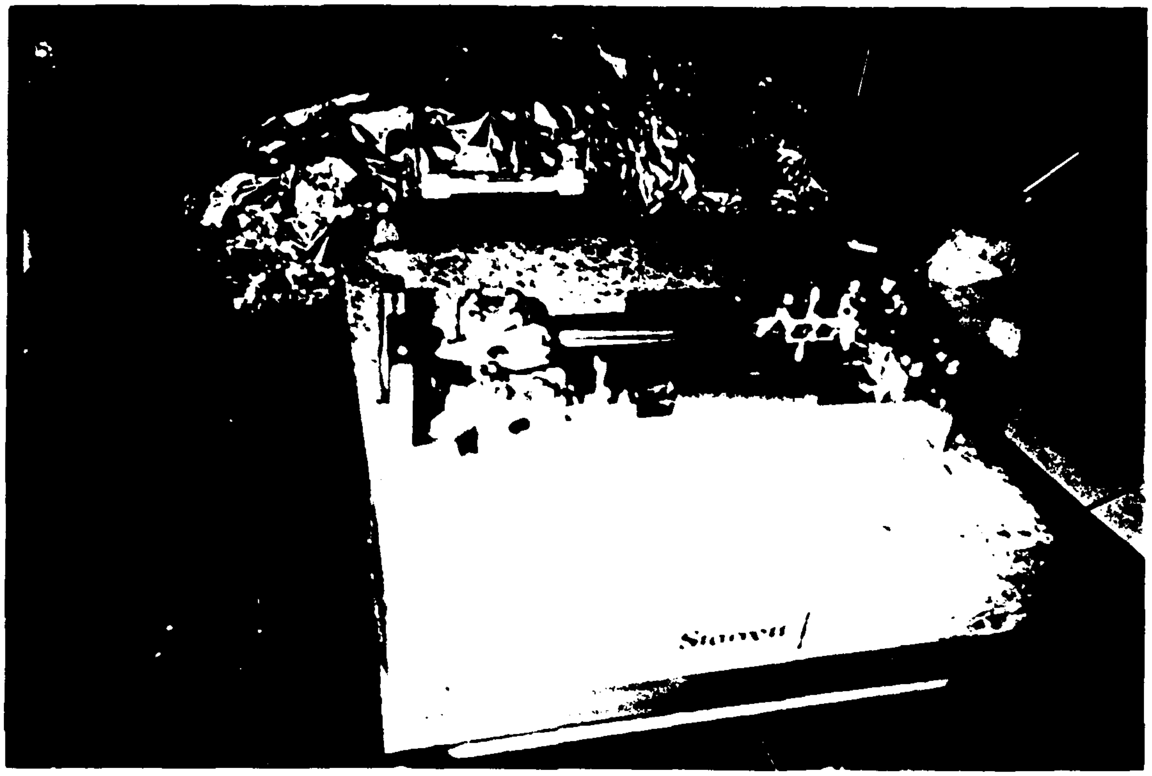

Figure 7

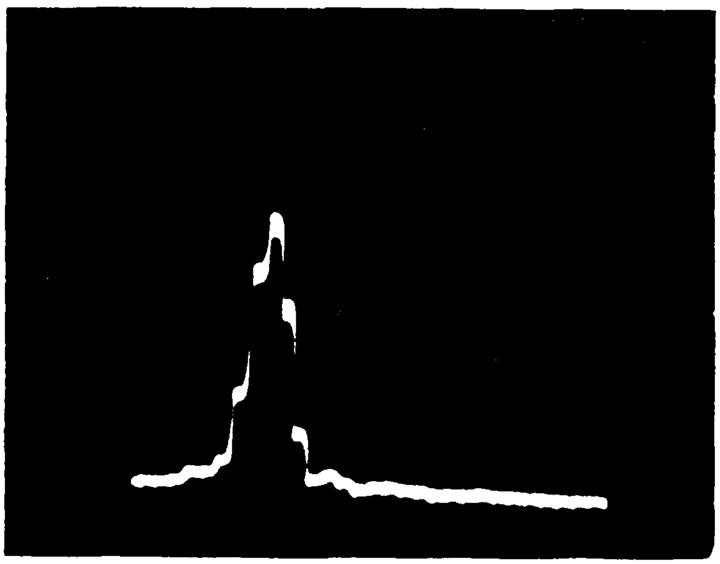

Figure 8

Figure 9

CHOPPER

MIRROR CHAMBER

DIFFERENTIAL SECTION

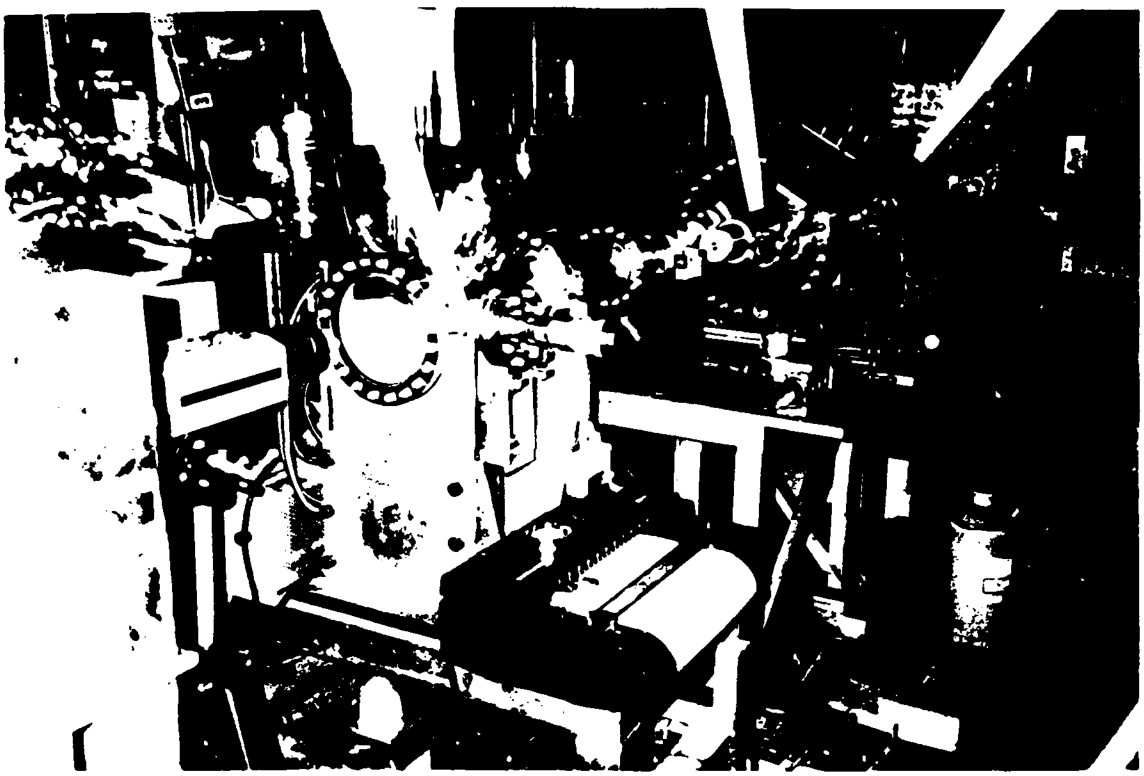

Figure 10a

MIRROR INSTALLED IN
MIRROR CHAMBER
(FORK WITH ALIGNMENT
MIRROR VISIBLE)

Figure 10b

MIRROR CHAMBER

EXTENSION NIPPLE WITH
PHOSPHORIZED VIEWPORT
FOR VIEWING DISPERSED
UNDULATOR SPECTRUM

Figure 10c

REFERENCE/ALIGNMENT

CRYSTAL

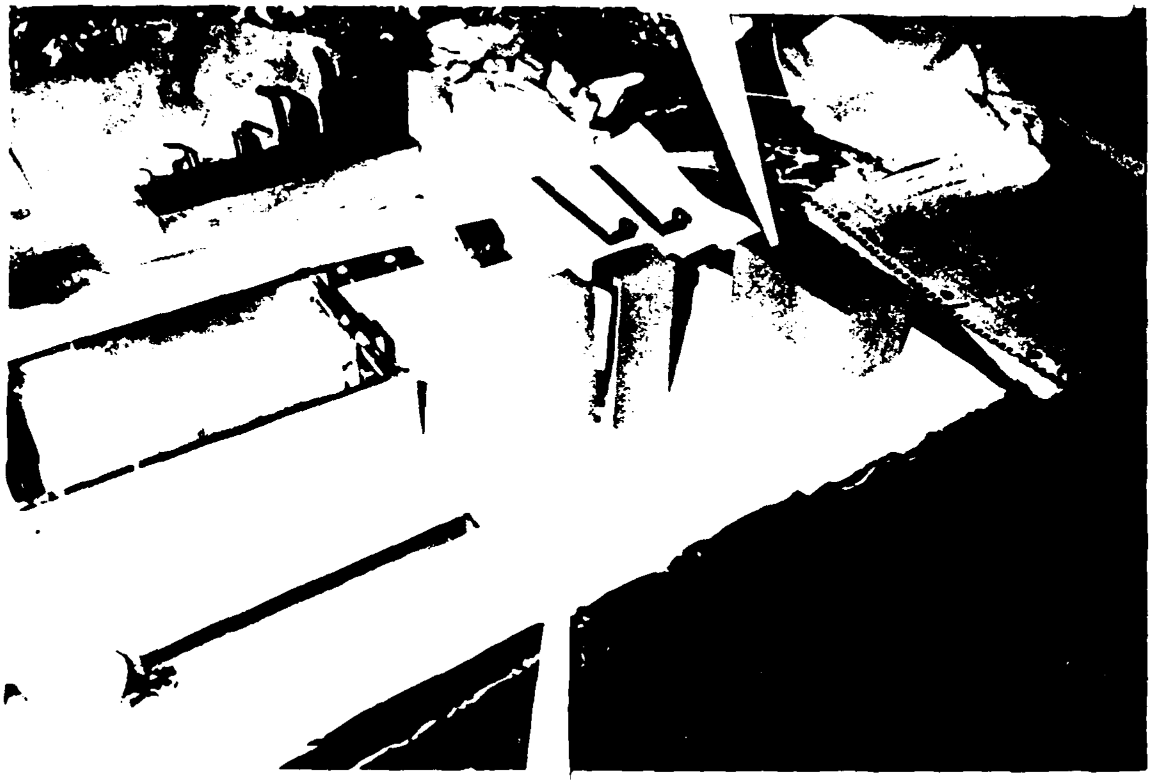

INTERFEROMETER CASING

MIRROR CRYSTALS

Figure 11

ADJUSTABLE
PHOSPHORIZED
STOP APERTURE
CARRIGE

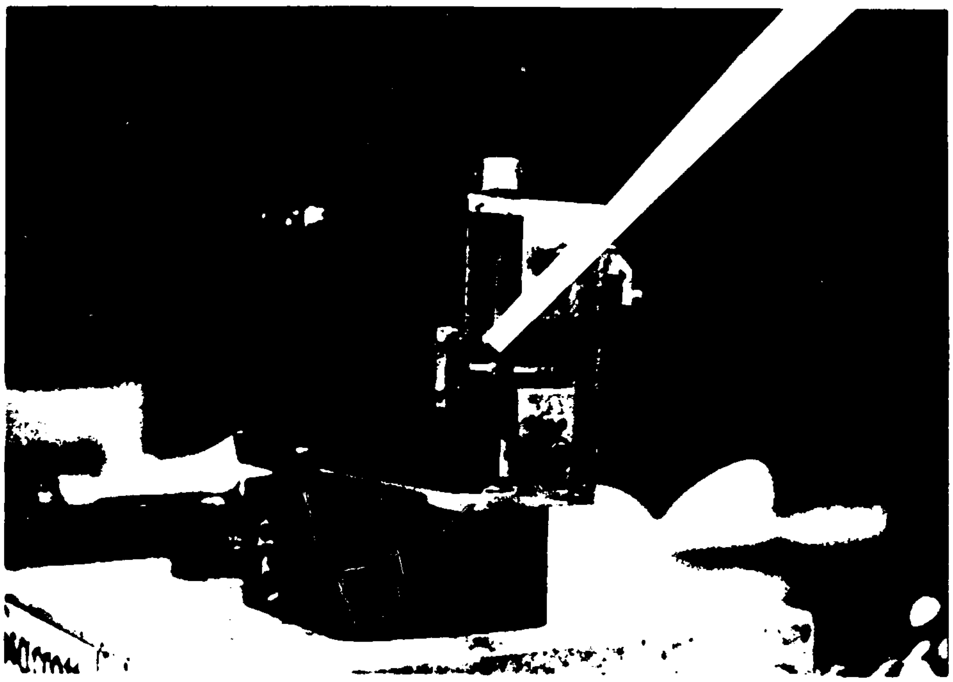

ASSEMBLED

INTERFEROMETER

Figure 12

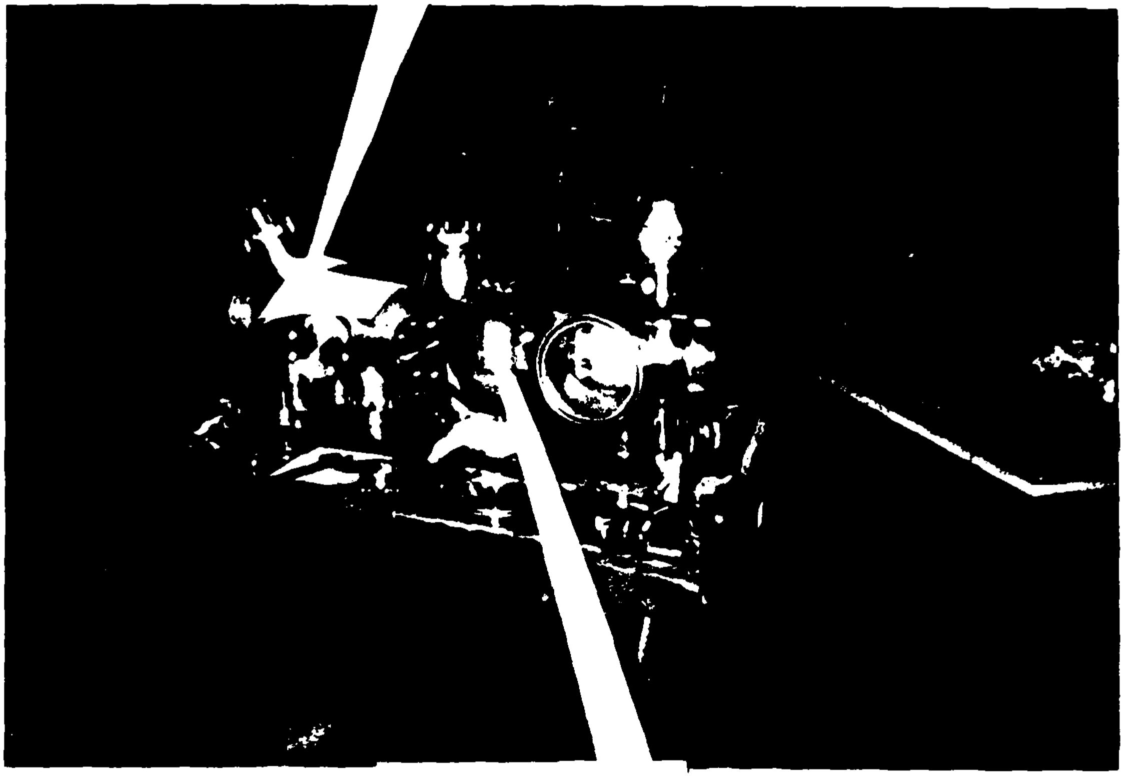

Figure 13

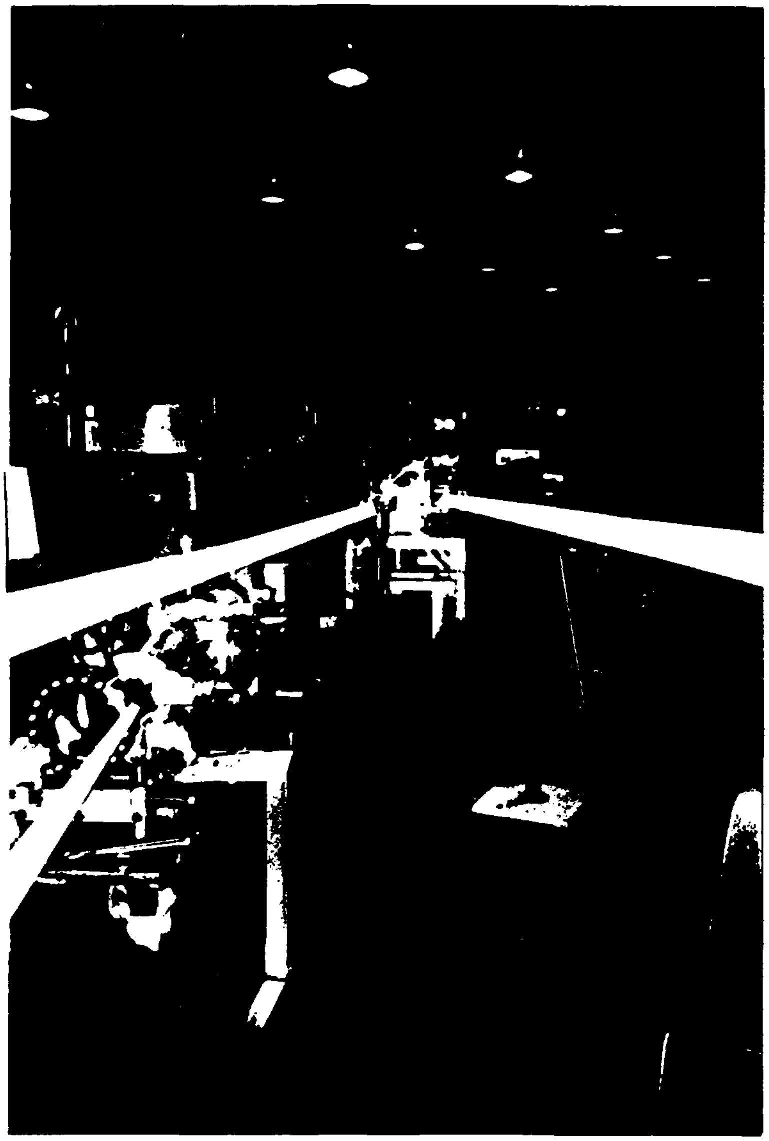
ADJUSTABLE SLIT ASSEMBLY IN MONOCHROMATOR EXIT PLANE
MIRROR CHAMBER
INTERFEROMETER CHAMBER

Figure 14

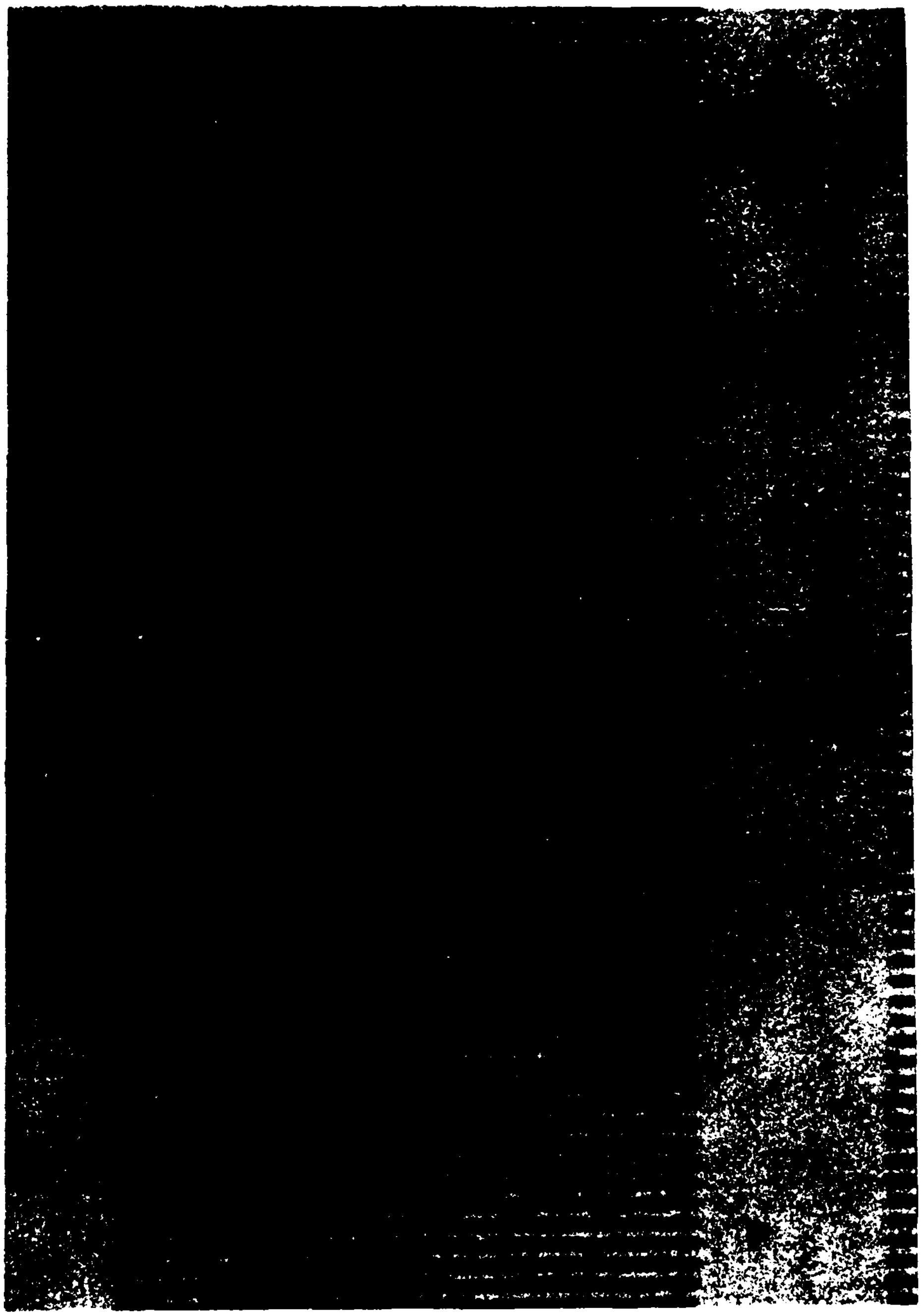

Figure 15

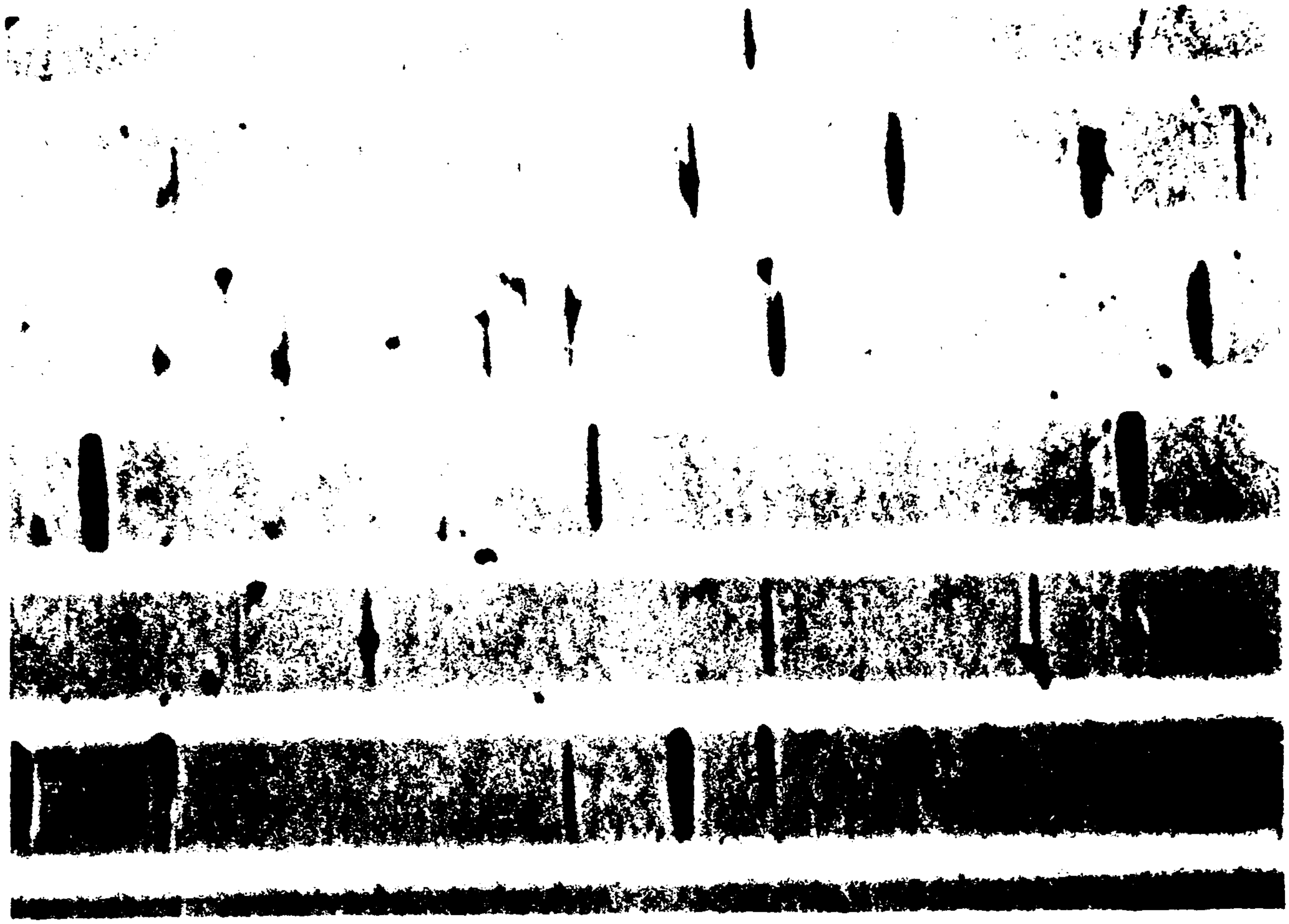

Figure 16a

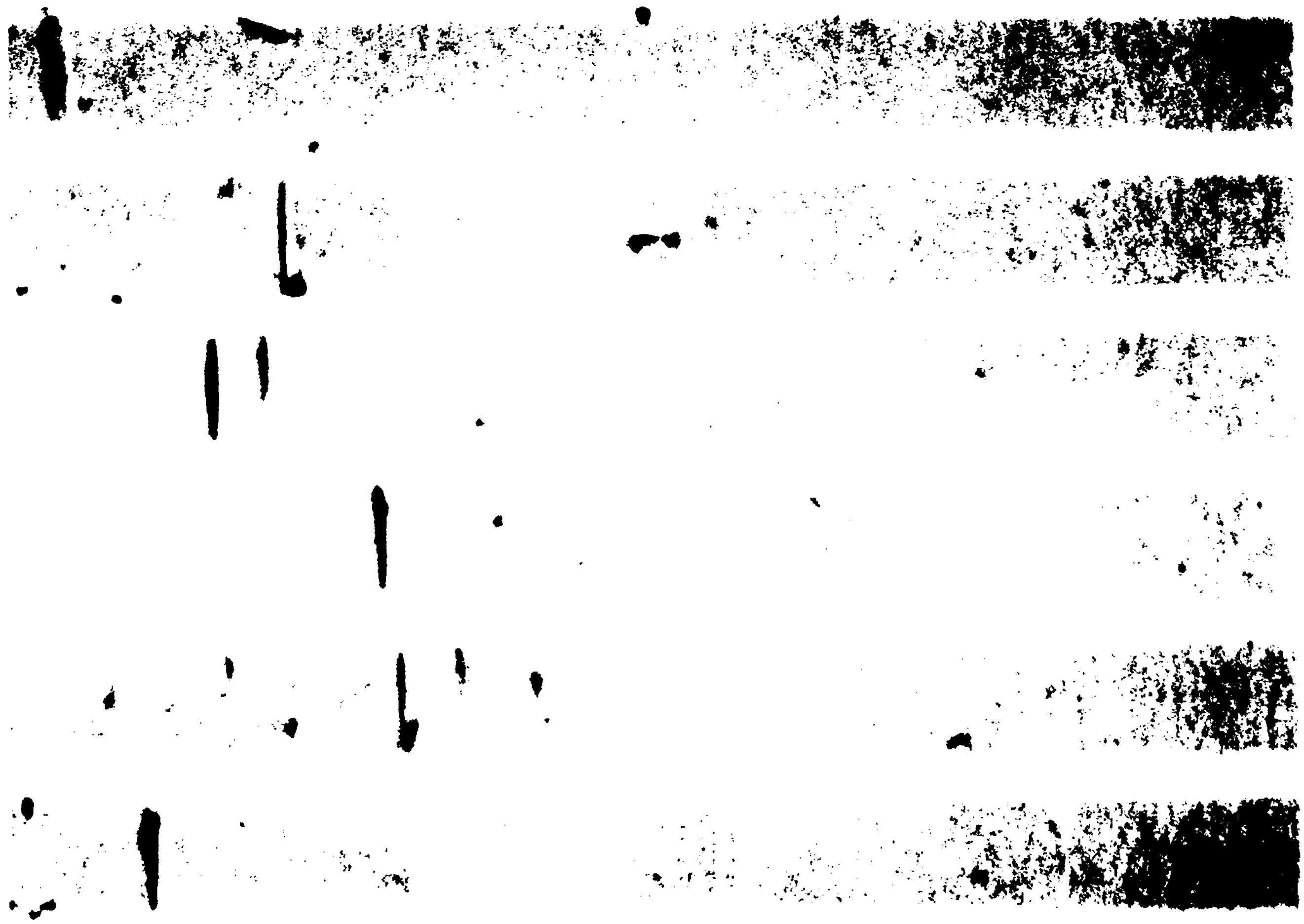

Figure 16b

Figure 17

Figure 18

END
5-89
DTIC